Fractal Structure of Polymer Interfaces

Richard P. Wool* and John M. Long

Department of Materials Science and Engineering, University of Illinois, 1304 West Green Street, Urbana, Illinois 61801

*Received January 15, 1993; Revised Manuscript Received May 25, 1993**

ABSTRACT: When diffusion occurs at an interface, the concentration profile $p(x, t)$ varies smoothly as a function of the one-dimensional depth x. However, when the diffusion process is viewed in two or three dimensions, the interface is not smooth and is very rough. The random nature of diffusion permits the formation of complex structures with fractal characteristics. In this paper, we use gradient percolation theory developed by Sapoval et al. to examine the structure and properties of diffuse interfaces formed by metallization of polymer substrates and welding of symmetric amorphous polymer interfaces. Gradient percolation separates the connected from the nonconnected region of the diffusion field. The edge of the connected region is the (fractal) diffusion front. We examine the ramified diffuse interface structure in terms of the diffusion front's width σ_f, length N_f, position X_f, breadth B_f, fractal dimension D, and "noise" in these properties, $\delta\sigma_f^2$, δN_f^2, δX_f^2, and δB_f^2, respectively, as a function of the diffusion length L_d. We obtained the following computer simulation and theoretical results: width, $\sigma_f \sim L_d^{1/D}$, $\delta\sigma_f^2 \sim L_d^{3/D}$; front length, $N_f \sim L_d^{1-1/D}$, $\delta N_f^2 \sim L_d^{2-1/D}$, $\delta N_f^2 \sim L_d^{2-1/D}$; position, $X_f \sim L_d$, $\delta X_f^2 \sim L_d^{2-1/D}$, breadth $B_f \approx 6\sigma_f$, $\delta B_f^2 \sim L_d^{2-1/D}$, where $D = {}^7/_4$. The simulation results compared very favorably with an experimental analysis of diffuse silver–polyimide interfaces. For welding of polymer–polymer interfaces, we examined the diffusion front for reptating chains of molecular weight M and found that the interface became fractal at diffusion distances L_d, greater than the radius of gyration $R_g \sim M^{1/2}$, and at times t, longer than the reptation time T_r. At $t < T_r$ and $L_d < R_g$, self-similarity was lost due to the correlated motion of the chains creating "gaps" in the interface. However, the interface was very rough and the diffusion front was determined by $N_f \sim L_d^d/M$, where d is the dimensionality (d = 2 or 3). When $L_d \gg R_g$, the polymer diffusion front behaved as the monomer case with $N_f \sim L_d^{1-1/D}$. The fractal nature of diffuse interfaces plays an important role in controlling the physical properties of polymer–polymer and polymer–metal interfaces.

Introduction

When diffusion occurs at an interface between two materials A and B, the concentration depth profile $p(x,t)$ of the A species in the B side varies smoothly as a function of the one-dimensional depth variable, x. However, when the diffusion process is viewed in two or three dimensions, the interface is not smooth and can be very rough. For example, Figure 1 shows a two-dimensional view of a monomer–monomer interface, a polymer–polymer interface (one side of interface), and a polymer–metal interface.[1-3] The random nature of diffusion permits the formation of complex structures with fractal characteristics. The diffusion field in each case is divided into two parts: the part nearest the origin (dark) is connected to itself through a percolation criterion, and the nonconnected part involves small clusters of diffusing molecules which are not connected to the source of diffusion. The frontier separating the connected from the nonconnected regions is called the "diffusion front" by Sapoval, Rosso, and Gouyet.[3-8] The diffusion front has fractal character and provides an elegant method of describing the naturally rough structure of interfaces. The roughness and position of the diffusion front vary as a function of the average monomer interdiffusion depth, $X(t)$. Consequently, properties which are sensitive to connectivity, e.g., adhesion strength, mechanical modulus, thermal expansion, and electrical conductivity, have a strong dependence on this type of structure. The concepts presented in this paper have application to polymer interfaces but are of general importance to any diffuse interface.

In this paper, we utilize the approach of Sapoval et al. in describing the fractal structure of interfaces. The concentration profile and structures shown in Figure 1 can be understood in terms of gradient percolation concepts which provide a natural basis for describing the ramified (rough) and fractal characteristics of polymer–polymer interfaces. We first analyze gradient percolation using computer simulation and then apply the characterization methodologies to a silver-polyimide interface. Finally, we examine the fractal structure of a polymer–polymer interface simulated by reptation diffusion.

Gradient Percolation

Consider the two-dimensional lattice diffusion of A atoms (shown in Figure 2) into B atoms (not shown) as discussed by Sapoval et al.[4-8] The concentration profile $p(x)$ of A atoms is given by the Fickian result,

$$p(x) = \mathrm{erfc}(x/L_d) \tag{1}$$

where $L_d = 2(D_0t)^{1/2}$ is the Einstein diffusion length at time t, with diffusion coefficient D_0. The diffusion front (heavy line in Figure 2) is defined by those A atoms which are connected to the diffusion source at $x = 0$ via other A atoms and have an empty first or second B neighbor which is itself connected to the source of B atoms. The interface with a diffusion front is seen to consist of solid regions with lakes or holes leading down to the "seashore" and unconnected islands of A atoms in the B "sea". The presence of holes and the connectedness between atoms in the interface are important in determining electrical and mechanical properties of the interface.

Figures 3–5 show larger scale (512 × 512 lattice) computer simulations of the diffusion front at diffusion lengths L_d = 256, 512, and 10 240 lattice units, respectively. The diffusion profiles were generated using the Fickian profile (equation 1) such that the concentration of A atoms, $p = 1$, is highest at the bottom of each figure (black) at $x = 0$ and decreases toward the top (white), $x \gg 0$. At any interdiffusion depth x, an A atom is placed with probability p, and the site is given a color depending on its occupation

* Abstract published in *Advance ACS Abstracts*, August 15, 1993.

0024-9297/93/2226-5227$04.00/0

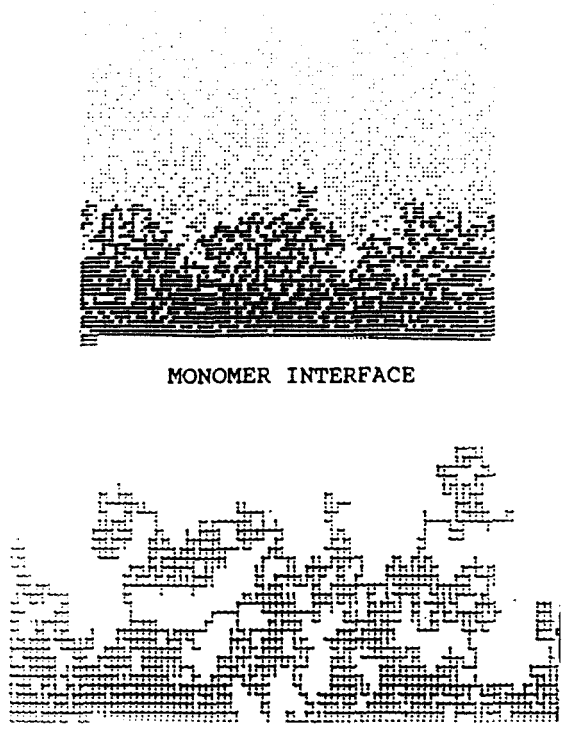

Figure 1. Ramified fractal nature of diffuse interfaces shown for (top) a computer-simulated 2d monomer–monomer interface where the dark region represents the connected monomers on one side of the interface, (middle) a simulated 2d random coil polymer interface at the reptation time, and (bottom) electrochemically deposited silver diffusing in polyimide with the nonconnected atoms removed to show the fractal diffusion front of the connected metal atoms.

and connectivity. The diffusion front (gray) becomes more extensive and ramified with increasing diffusion depth, L_d. The black to white shades represent the connected A atoms (black), A-atom clusters (white), and diffusion front (gray). The A atoms which are connected to the $x = 0$ plane are shown in black. The connectivity criterion was identical to that used for the percolation algorithm in Figure 2. If the A atoms were metal, the black region represents those atoms which could conduct electricity introduced at $x = 0$. One might argue for polymers that the black region represents the area connected by entanglements to the A side of the interface. The black region extends up to the percolation threshold concentration p_c, at position $x(p_c)$. At lower concentrations or diffusion distances, $x > x(p_c)$, we are below the percolation threshold and the connectivity is lost.

The white regions represent the clusters of A atoms which are not connected to the source at $x = 0$. The clusters are small at the top of the figure but increase in size in the vicinity of the percolating black region. Note that many white islands exist in the black region. These are A atoms which are surrounded by B atoms and therefore not connected to the A source at $x = 0$. If the B atoms were

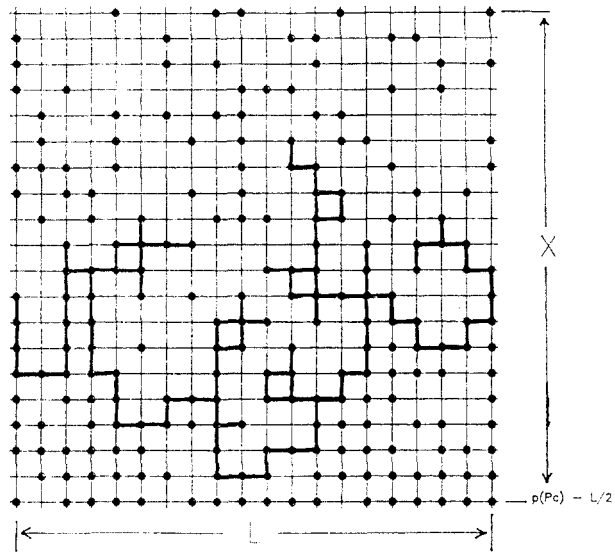

Figure 2. Gradient percolation where the diffusion of A atoms on a 2d lattice is shown. The concentration gradient decreases from the bottom to the top of figure. The bold line represents the diffusion front which separates the connected from the nonconnected A atoms (courtsey of Sapoval et al.[4]).

nonconducting, then the white A islands do not contribute to the black conduction zone.

The connected B zone extends down to the connected A zone, and the region where they meet is the diffusion front (gray). The diffusion front can also be understood as the frontier which separates the connected and nonconnected A atoms. The roughness and width of the diffusion front increase with diffusion length, and its fractal character becomes more apparent, e.g., comparing Figure 3 ($L_d = 256$) with Figure 5 ($L_d = 10\,240$). Note that, in Figure 5, the gray diffusion front contains many black islands; these represent conducting A atoms which are not in contact with B atoms but connect through the front. In the next section, the methods of characterizing the fractal nature of diffusion fronts are examined.

Characterization of Diffusion Fronts

The diffusion front of the interfaces shown in Figures 3–5 can be characterized by three macroscopic quantities: its position x_f, in the concentration gradient $p(x)$, its width σ_f, and the total number of particles on the front N_f.[4–8] The ramified character of the front can be described from the mass to radius relation,

$$M \sim R^D \tag{2}$$

where $D = {}^7/_4$ is the fractal dimension of the front in 2d.

Position of the Diffusion Front x_f. The concentration of particles at the mean front position x_f is identical to the percolation threshold[4–8] such that $p(x_f) = p_c$, where for site percolation $p_c = 0.593$. The simulation results for p_c are shown in Table I. The position of the front is proportional to the diffusion length L_d,[4] and for a 2d lattice with a Fickian error-function profile, we have from eq 1 at concentration p_c

$$x_f = 0.378L_d \tag{3}$$

or $L_d = 2.645x_f$. The error-function profile is similar to the linear profile used by Sapoval et al.[4] at large L_d values. However, the error-function profile is valuable at short diffusion distances, particularly when making a comparison with experimental data.

Sapoval et al.[4–8] have used the gradient percolation method as an accurate method of determining p_c from the

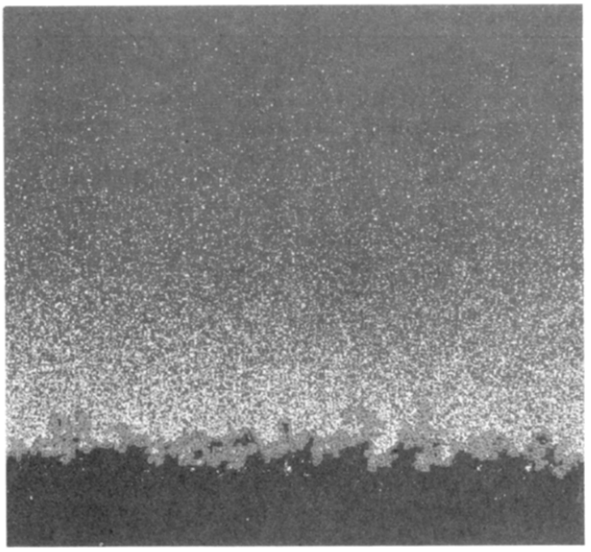

Figure 3. Gradient percolation simulation of atoms diffusing on a 512 × 512 lattice with a diffusion length $L_d = 256$. The gray region represents the diffusion front between the connected (black) and nonconnected (white) atoms.

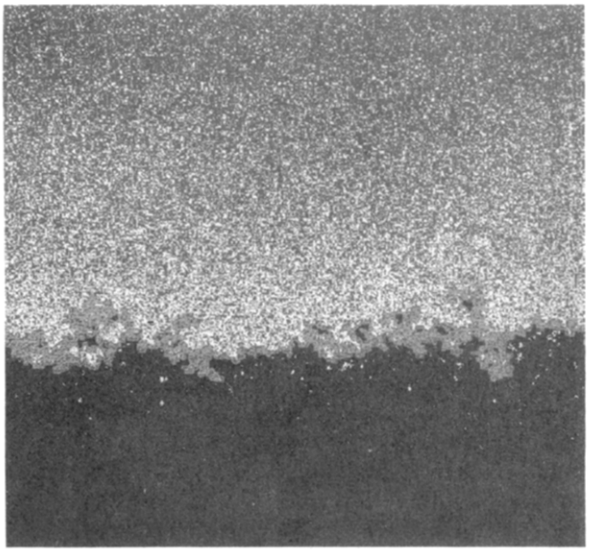

Figure 4. Gradient percolation of atoms with a diffusion length $L_d = 512$ on a 512^2 lattice.

front position. Considerable uncertainty in the p_c determination can arise with traditional percolation simulations done at constant p on finite size lattices.

Fractal Dimension of the Diffusion Front, *D*. The fractal dimension D of the front shown in Figure 5 (L_d = 10 240) was determined from the slope of the plot of log mass versus log radius, as shown in Figure 6. We obtained $D = 1.76$, which is in excellent agreement with the prediction of Sapoval et al. The mass of the front was measured as follows. Circles of radius R with their centers placed on the $x(p_c)$ line were drawn (by computer). The number of front particles (gray) contained in each circle was determined as a function of R, and the procedure was averaged over many locations on the diffusion front x_f line. The procedure was repeated at least 50 times for different fronts generated at the same diffusion length. The analysis is applicable to radii in the range $R \ll \sigma_f$. When R exceeds the width of the front, then $M \sim R^1$ and $D = 1$, as shown in Figure 6 with $L_d = 128$ and $R > 20$ lattice units.

We examined the fractal dimension using lattices of size 256^2, 512^2, and 1024^2 and diffusion lengths up to 10^4

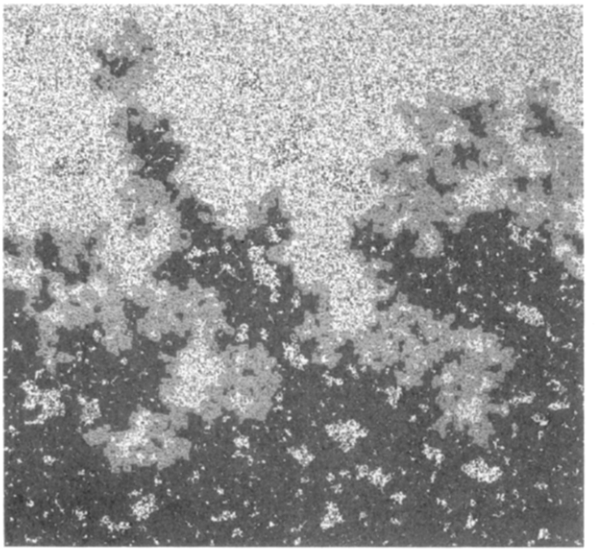

Figure 5. Gradient percolation of atoms with a diffusion length L_d = 10 240 on a 512^2 lattice.

lattice units. Periodic boundary conditions were used on the lateral sides. We found that D was independent of diffusion length when $R < \sigma_f$, as shown in Figure 7 for the 1024^2 lattice. In the latter case we obtained $D = 1.754 \pm 0.079$, where the standard deviation of 0.079 was obtained from an average of 50 runs at each diffusion length. The scatter in the data shown in Figure 7 was found to be constant with increasing diffusion length.

The fractal dimension appeared to be bounded by the range $1.675 \leq D \leq 1.833$. The value of $D = 1.833$ might correspond to portions of the front which have internal cluster character ($D_c = 1.89$), and the lower value of D = 1.675 may correspond to more open structures similar to diffusion limited aggregation and viscous fingering with $D \approx 1.64$. However, we should be cautious about interpreting the scatter of the diffusion front dimension in terms of other fractal structures. A small lattice size dependence on D was observed where slightly lower D values (ca. 1.734) were obtained with 256^2 compared to the 1024^2 lattice (Table I).

We conclude that the value of $D = {}^7/_4$ predicted from percolation theory is an excellent convergence limit at high lattice size. It was suggested by Sapoval et al.[4] that the fractal dimension of the front is related to the critical exponent υ, for 2d percolation via

$$D = (1 + \upsilon)/\upsilon \tag{4}$$

Since $\upsilon = {}^4/_3$, eq 4 predicts that $D = {}^7/_4$.

Width of the Diffusion Front, σ_f. As is evident from Figures 3–5, the width of the front σ_f increases with diffusion length L_d. Sapoval et al.[4] analyze this problem with the following arguments [reviewed in ref 8]. As $p(x)$ approaches p_c, the cluster size of A atoms (white in Figure 5) begins to approach the width of the front. Thus the main length scale is related to the correlation length evaluated at $x_f \pm \sigma_f$. The concentration gradient dp/dx prevents σ_f from becoming infinitely large at p_c. However, as the diffusion depth increases and the concentration gradient decreases, the width of the front will increase toward infinity and converge on the normal percolation case with a uniform average concentration near p_c. The average cluster size ζ is related to the concentration p by

$$\zeta = [p - p_c]^{-\upsilon} \tag{5}$$

where p_c is the percolation threshold and υ is the critical exponent.

Table I. Analysis of Diffusion Fronts

parameter	$Y = AL_d^{\alpha}$	256^2	512^2	1024^2	theory	sapoval
front width σ_f	A_f	0.859	0.608	0.597	ca. 1	0.46
	$\alpha(\sigma_f)$	0.479	0.521	0.544	0.571	0.57 ± 0.01
width noise $\delta\sigma_f^2$	A	1.56×10^{-3}	10^{-4}	2.46×10^{-5}	$0.06/L$	
	α	1.469	1.621	1.764	1.71	
length of front N_f	$A(N_f)$	1.074	0.949	0.918	0.97	0.96
	$\alpha(N_f)$	0.409	0.427	0.430	0.43	0.425
length noise δN_f^2	A	0.404	0.240	0.200	ca. 1	ca. 2
	α	1.333	1.400	1.437	1.428	1.5 ± 0.05
front position X_f	A	0.361	0.371	0.376	0.378	0.378
	α	0	0	0	0	0
position noise δX_f^2	$A \times 10^3$	6.63	2.02	2.44		
	α	1.462	1.400	1.472	1.428	
fractal dimension D	D	1.734	1.741	1.753	1.75	1.76
	δD	0.089	0.079	0.079	0.000	0.02
frontier breadth B	$A(B)$	6.962	5.98	5.366		
	$\alpha(B)$	0.404	0.449	0.479		
breadth noise δB^2	A	0.146	0.055	0.012		
	α	1.126	1.254	1.432	1.428	
threshold p_c	p_c	0.598	0.596	0.594	0.593	0.593
	δp_c	0.015	0.010	0.007	0.000	0.000

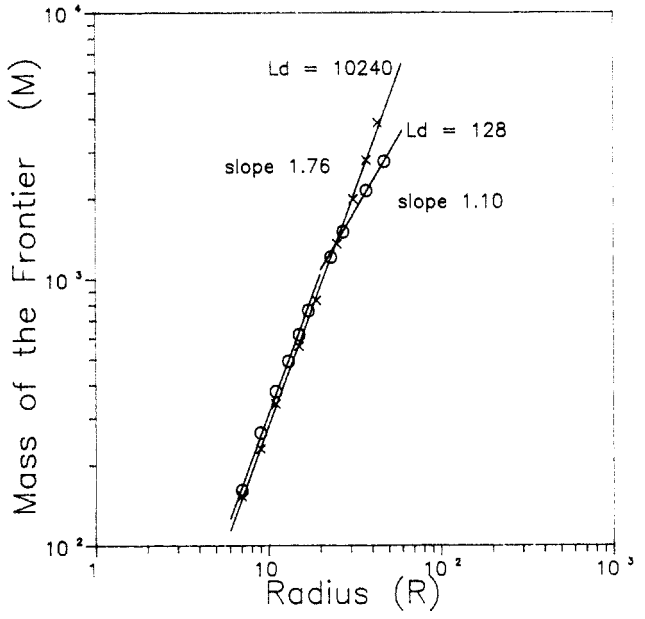

Figure 6. Mass of diffusion front vs radius which determines the fractal dimension D: (–×–) L_d = 10 240 from Figure 5; (–○–) L_d = 128.

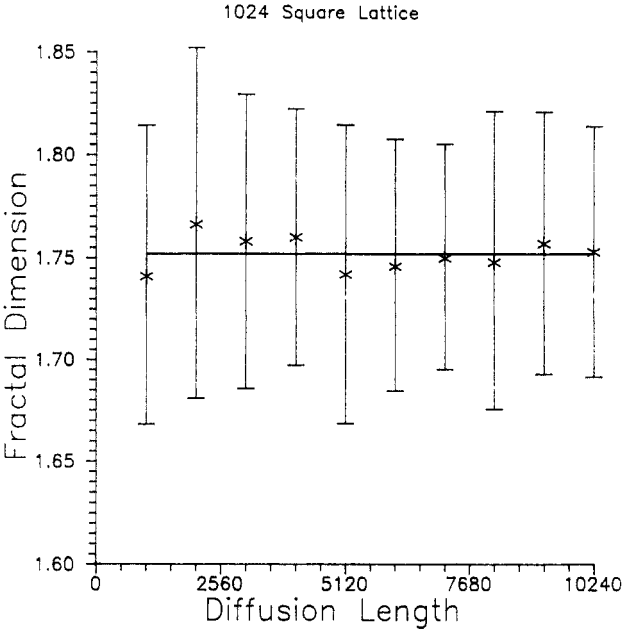

Figure 7. Fractal dimension D vs diffusion length L_d for a 1024^2 lattice.

Using eq 5 for the cluster size as a function of $p(x)$ and expanding $p(x)$ around x_f, they obtain[4]

$$\sigma_f \sim [p(x_f \pm \sigma_f) - p_c]^{-\upsilon} \tag{6}$$

$$\sigma_f \approx [\sigma_f\{dp/dx\}x_f]^{-\upsilon} \tag{7}$$

in which the proportionality constants are on the order of unity.

The concentration gradient dp/dx is inversely proportional to the diffusion length L_d. From eq 1, $dp/dx(x_f) = 0.997/L_d$. Therefore, the diffusion length dependence of σ_f is

$$\sigma_f \approx L_d^{\alpha(\sigma)} \tag{8}$$

where the exponent $\alpha(\sigma)$ is related to the percolation exponent υ, by

$$\alpha(\sigma) = \upsilon/(\upsilon + 1) \tag{9}$$

When $\upsilon = {}^4/_3$ in 2d, then $\alpha(\sigma) = 1/D = {}^4/_7$ and

$$\sigma_f \approx L_d^{0.57} \tag{10}$$

Computer simulations by Sapoval et al.[4] gave excellent support to eq 10. Results of our computer simulations are shown in Figure 8 for the 1024^2 lattice (and Table I) where we obtain

$$\sigma_f = 0.60L_d^{0.54} \tag{11}$$

which is in close agreement with the theoretical prediction. In this case, the standard deviation $\delta\sigma_f$ increases with L_d from $\delta\sigma_f$ = 2.2 at L_d = 1024 to $\delta\sigma_f$ = 16.75 at L_d = 10 240. This is to be expected since the fluctuations in the position of the diffusion front are also increasing with L_d. Results with other lattices are listed in Table I.

Span of the Diffusion Front, *B*. The span of the front $B = 2|x_m - x_f|$ was determined where x_m is the largest value of the diffusion depth which still contains the front. B is essentially the full width of the diffusion front in the depth direction while σ_f describes the standard deviation. The span has significance in terms of designing electronic devices which encapsulate the front without leakage.

If $p_f(x)$ is the Gaussian concentration profile of the front, then the profile centered about x_f is determined in terms of N_f and B as

$$p_f(x) = [N_f/(\sigma_f L\sqrt{2\pi})] \exp[-(x - x_f)^2/2\sigma_f^2] \tag{12}$$

Since $B = 2(x_m - x_f)$, the relation between B and σ_f is

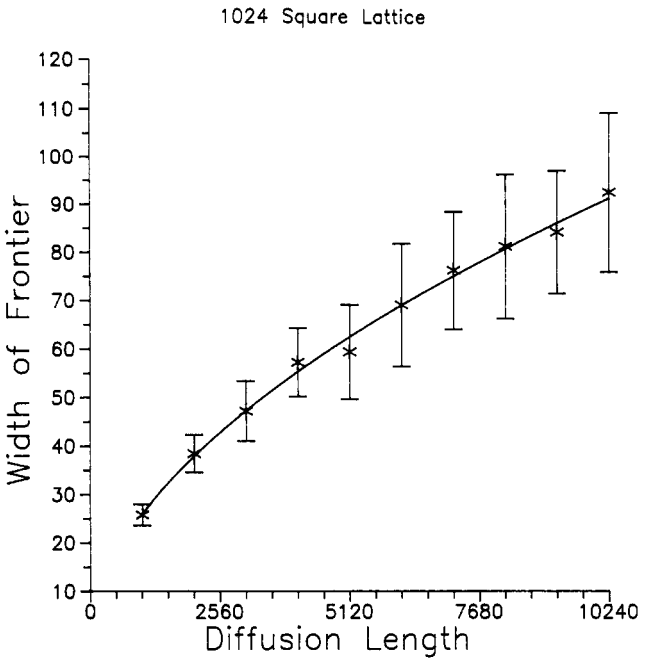

Figure 8. Diffusion front width σ_f vs diffusion length L_d for a 1024^2 lattice. The simulation was done on a $1{,}024^2$ lattice. The solid line is given by the power law. $\sigma_f = 0.597L_d^{0.544}$. The error bar height represents the standard deviation $\delta\sigma_f$.

obtained as

$$p_f(x_m) = q/L \tag{13}$$

as the ratio

$$B/\sigma_f = 2\sqrt{2}[\ln N_f/(q\sigma_f\sqrt{2\pi})]^{1/2} \tag{14}$$

where q is the number of atoms which can be detected on the smallest cluster on the outer regions of the diffusion front. Thus q should be on the order of (but greater than) unity.

Substituting for the diffusion length dependence of N_f and σ_f on the right-hand side of eq 14, we obtain

$$B/\sigma_f = 2\sqrt{2}\{\ln[0.83L/(qL_d^{1/7})]\}^{1/2} \tag{15}$$

Thus, the span B is not directly proportional to the width σ_f, as might have been expected, but is modified by the $L_d^{1/7}$ factor on the right-hand side.

The computer simulation gives B/σ_f = 4.82, 5.97, and 5.72 for the 256, 512, and 1024 lattices, respectively, with L_d = 1024, and B/σ_f = 4.05, 5.05, and 4.93 with L_d = 10 240, respectively. Analysis of this data suggests that a value of $q \approx 6$ is required to obtain agreement between simulation and eq 15. The ratio B/σ_f determined from simulations is expected to depend on the lattice size since larger lattices have a higher probability of producing larger B values. With increasing diffusion length L_d, the ratio B/σ_f converges slowly to a value of $2\sqrt{2}$.

The "noise" in the width of the diffusion front can be expressed as the square of the standard deviation $\delta\sigma^2$ and was found to behave for the 1024^2 lattice as

$$\delta\sigma_f^2 = 2.5 \times 10^{-5}L_d^{1.76} \tag{16}$$

The exponent was found to be lower with the other lattices (Table I), and the front factor is on the order of $1/L^2$. This result will be discussed with other features of the noise in the diffusion front in a later section.

Number of Atoms on the Diffusion Front, N_f. The number of atoms on the front, N_f, is a very important parameter and readily quantifies the roughness of the interface in many practical situations. For example, in Figures 3–5, we would like to know how the length of the diffusion front (gray line) changes with diffusion length L_d. By examining Figures 3–5, we see that N_f increases with diffusion length. The exact dependence can be derived as follows:[4]

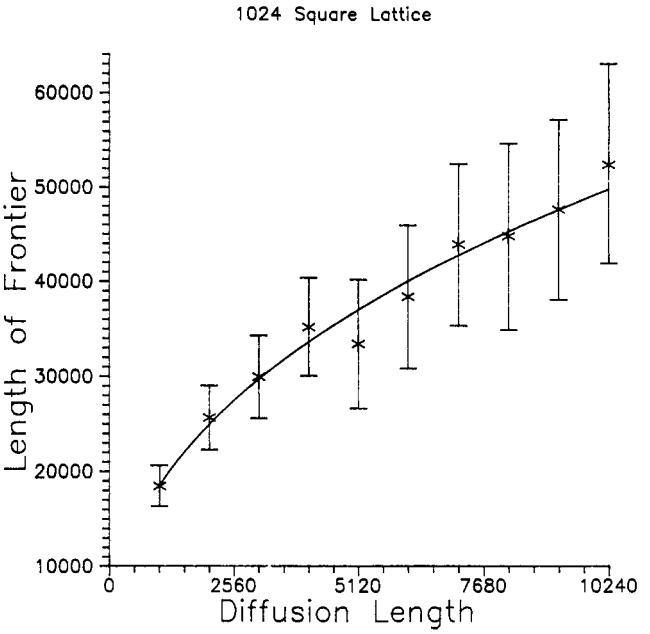

Figure 9. Length of frontier N_f vs diffusion length L_d. The error bar heights represent the standard deviation δN_f, for a minimum of 50 simulations on a $1{,}024^2$ lattice.

Consider a square "box" on the diffusion front of length σ_f. Because the front is fractal, the box contains σ_f^D atoms, as per eq 2. If the length of the interface is the lattice length L, then the interface contains L/σ_f independent fractal boxes and the total number of atoms on the front is

$$N_f \sim L\sigma_f^{D-1} \tag{17}$$

where the proportionality constant is near unity. Substituting for σ_f from eq 10, then

$$N_f \sim LL_d^{\alpha(N)} \tag{18}$$

where the exponent $\alpha(N)$ is

$$\alpha(N) = (D-1)(\upsilon/\upsilon + 1) \tag{19}$$

In two dimensions, $D = {}^7/_4$ and $\upsilon = {}^4/_3$ such that $\alpha(N) = (1 - 1/D) = {}^3/_7$ and

$$N_f \sim LL_d^{0.43} \tag{20}$$

Figure 9 shows our computer simulation analysis of this relation where the length of the frontier N_f is plotted as a function of the diffusion length L_d, for the 1024^2 lattice. The solid line in Figure 9 is given by the power law

$$N_f = 940.5L_d^{0.43} \tag{21}$$

which is in excellent agreement with theory. The front factor of 940 in eq 21 is approximately equal to the lattice dimension (1024) as predicted by Sapoval et al.[4] The front factor can be normalized by the lattice dimension as 940/1024 = 0.92. The standard deviation, δN_f, is also strongly dependent on L_d and changes from 2163 at L_d = 1024 to 10 704 at L_d = 10 240.

The interface roughness can be described by the number $S = N_f/L$. If we take a box on the front of length σ_f containing σ_f^D particles, then we have the simple relation

(see Table I) that

$$\sigma_f^D = 0.4L_d \tag{22}$$

Since $S = \sigma_f^D/\sigma_f$ and $B \approx 6\sigma_f$, the interface roughness number is conveniently obtained in terms of diffusion observables as

$$S = 2.4L_d/B \tag{23}$$

This number has been referred as the "Sapoval number" and is based on the peculiarity that the number of particles in a box of width σ_f is proportional to the diffusion length, as expressed by eq 22. The actual number of particles on the front is related to S and the lattice length L by $N_f = SL$.

Dynamics and Noise of the Diffusion Front. If we examine the diffusion front (gray line) in Figure 5, it becomes apparent that small motions of single atoms on the front can disconnect or connect large clusters and dramatically alter the position of the front. For example, a cluster containing σ_f^D atoms can be connected or disconnected from the front by the motion of a single atom.

The dynamical properties of the diffusion front were examined by Sapoval, Rosso, Gouyet, and Colonna.[10] They note that the most remarkable feature about front fluctuations is their very high frequency. If Θ is the average jump time for a particle in the lattice, it is not necessary to wait this time for a jump to occur somewhere on the front but rather a much shorter time, Θ/N_f.

$\delta N_f(t)^2$ is defined as the square of the change of the number of points on the frontier in the time interval t,

$$\delta N_f(t)^2 = \langle N_f(t) - N_f(0)\rangle^2 \tag{24}$$

At short times, the fluctuations follow the law

$$\delta N_f(t)^2 \sim t^{2H} \tag{25}$$

where $H = {}^1/_2$ is the Hurst exponent corresponding to $1/f^2$ noise at high frequency. At longer times and lower frequencies, they find that the fluctuations stabilize. Above a crossover time t_c, $H = 0$, corresponding to a white spectrum.

The variation of $\delta N_f(t)^2$ in the low-frequency limit at $t > \Theta$ can be understood as follows.[10] The frontier is treated as L/σ_f independent percolating boxes of side σ_f, where each box represents the average cluster size which can be added or subtracted from the frontier. Since each box is fractal, it contains σ_f^D particles and the total fluctuation is

$$\delta N_f(t)^2 = (L/\sigma_f)\sigma_f^{2D} \tag{26}$$

Substituting for σ_f as a function of L_d, they obtain

$$\delta N_f(t)^2 = LL_d^{10/7} \tag{27}$$

which is independent of time at $t > t_c$. Their dynamic simulation gave an exponent of 1.5 ± 0.05, which compares with the theoretical value ${}^{10}/_7 = 1.428$.

We examined the dynamics prediction in eq 27 using our static simulations by assuming that an observer in a box of length σ_f when moved along the frontier to the next box will see fluctuations corresponding to the standard deviation of N_f. In Figure 9, the standard deviation δN_f (average of 50 runs per diffusion length), represented by the error bars, increases with diffusion length for $L = 1024$ lattice. A plot of δN_f^2 versus L_d in Figure 10 gave

$$\delta N_f^2(1024) = 0.2LL_d^{1.437} \tag{28}$$

For the 512^2 lattice, a similar analysis gives an exponent of 1.416 (Table I). The exponents of 1.437 and 1.416 are

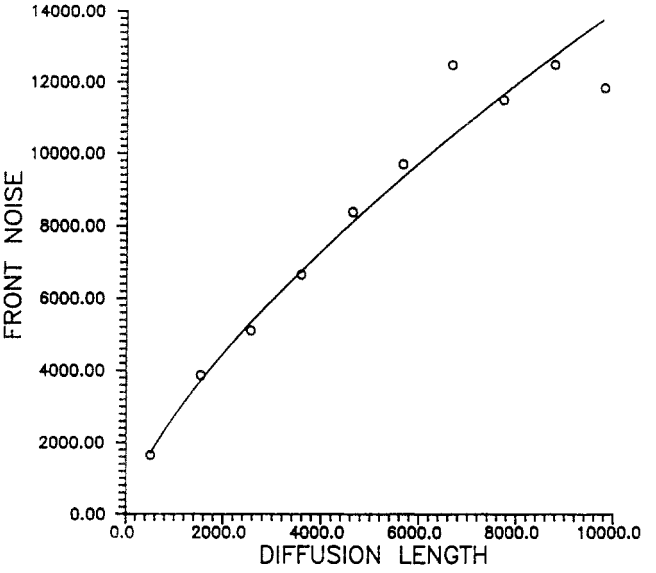

Figure 10. Frontier length noise δN_f vs diffusion length L_d. The solid line through the data points was determined by the power law fit, $\delta N_f = 14.3692L_d^{0.7184}$.

in very good agreement with the theoretical exponent of ${}^{10}/_7 = 1.428$. The front factor in this analysis is on the order of unity as predicted by Sapoval et al.

The fluctuations in the front width $\delta\sigma_f^2$, can be obtained by taking the derivative $\delta N_f/\delta\sigma_f$ of the relation $N_f \approx 2L\sigma_f^{D-1}$ and solving for $\delta\sigma_f^2$,

$$\delta\sigma_f^2 = \delta N_f^2/[4(D-1)^2L^2\sigma_f^{2(D-2)}] \tag{29}$$

Substituting both for δN_f^2 from eq 27 and for the diffusion length dependence of σ_f from eq 10, we obtain the diffusion length dependence of the width noise as

$$\delta\sigma_f^2 = 0.06/L\,L_d^{12/7} \tag{30}$$

The exponent of ${}^{12}/_7$ is in good agreement with the computer simulation with $L = 1024$ (Table I). The front factors which are proportional to $1/L$ are of the correct order of magnitude and are predicted by eq 30 to be 2.3×10^{-4}, 1.17×10^{-4}, and 5.8×10^{-5}, for the 256, 512, and 1024 lattices, respectively.

The "geometrical" nature of the noise in the diffusion front is surprisingly large considering the smooth advance of the average position of the front. The fluctuations δN_f may have interesting physical consequences; for example, large impedance fluctuations can occur in electrical contacts. The ability to control the diffusion front roughness (N_f) of a polymer–metal interface and its molecular connectivity has interesting implications for the mechanical and electrical property development of composites and electronic material interfaces. Roughness promotes mechanical interlocking, but fractal characteristics with holes could reduce electrical conductance and affect signal speed in the metal layer. The thickness of the conducting strip is determined by the position of the fractal diffusion front. In superconductor–metal interfaces, the chemical potential difference seen by the Cooper pair of electrons causes a splitting such that one electron travels across the planar interface into the normal metal conductor and the other is reflected back into the superconductor. This phenomenon is known as the Andreev reflection and is expected to be significantly altered by the presence of a fractal rough interface where the metal has diffused into the superconductor.

The fractal analysis of interfaces has been found useful by us for the examination of structure development at

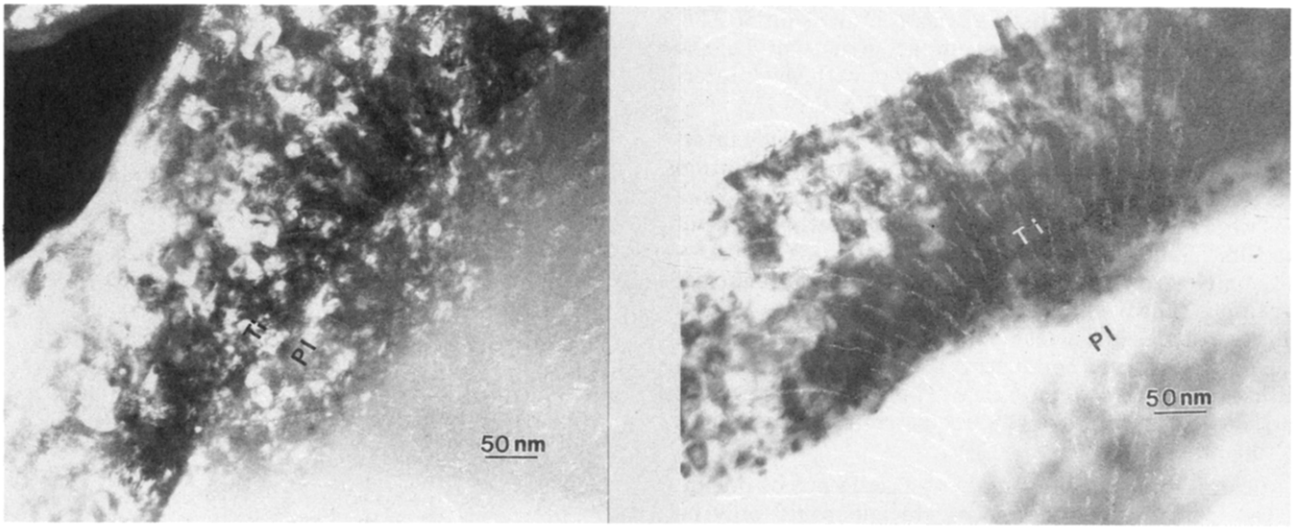

Figure 11. Transmission electron micrographs of a titanium–polyimide interface. The interface was formed by metallization of the PI substrate at 175 °C. The interface was subsequently annealed at 320 °C in deuterium (760 torr). Diffusion of the Ti in the PI phase is indicated (courtsey of Robertson et al.[14]).

reacting polymer–cement interfaces[11] and for the investigation of biodegradation of composites containing degradable and nondegradable components, e.g., starch and polyethylene (PE) blends. Biodegradation of such blends involves a percolation invasion process for materials in which the starch molecules are uniformly distributed in the PE matrix.[12,13] However, when flow-induced concentration profiles develop, the starch near the surface is removed by microbes while the remaining material is encapsulated within the PE matrix. The surface separating the accessed material from the encapsulated material is similar to the fractal diffusion front shown in Figure 5.

Polymer–Metal Interfaces

The structure of polymer–metal interfaces was explored using computer simulation experiments and image analysis of transmission electron micrographs. As a starting point, a computer simulation was developed using gradient percolation. The simulation was then used to study the effects of lattice size and diffusion length on the behavior of the fractal dimension of diffusion fronts and other associated parameters. Once we were satisfied that the simulation was behaving appropriately, we used it to examine the fractal dimension of a diffuse polyimide–silver (PI–Ag) interface.

Fractal Polymer–Metal Interfaces. Ordinarily, one forms a featureless polymer–metal interface by depositing the polymer on a flat metal surface. However, in vapor metallization processes, chemical vapor deposition, plasma-assisted vapor chemical deposition, and diffusion-controlled metallization, the metal atoms can diffuse considerable distances into the polymer substrate. This process is commonly used in the manufacture of very large systems integrated (VLSI), i.e., high-performance electronic materials and integrated circuits. For example, Figure 11 shows a 2500-Å titanium strip which was vapor deposited on a polyimide (MDA–ODA) substrate by Robertson et al.[14] The Ti–PI interface is diffuse, with the Ti diffusing up to 1000 Å in the PI. The structure of the diffuse interface depends on the deposition conditions and annealing treatments. Metal atoms which complex strongly to the PI are not expected to form deep diffuse layers.[15] Similar observations of diffuse interfaces were made using copper, silver, tungsten, and nickel.[14,15]

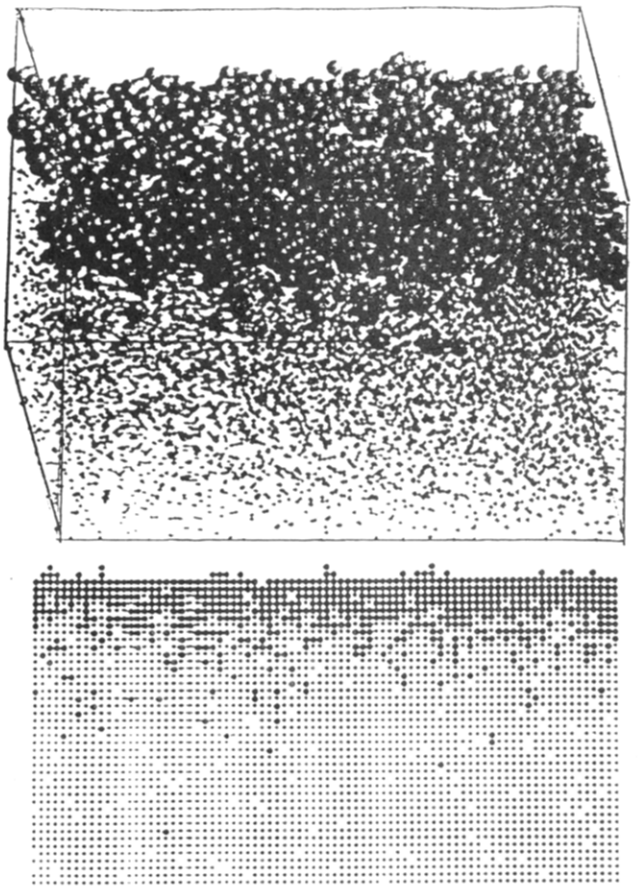

Figure 12. Top: Three-dimensional view, at an angle to the top film surface after deposition of a quarter monolayer of metal atoms. The metal atoms are shown as large spheres. Bottom: Metal atom penetration profile into the polymer film just after initial metallization (courtsey of Silverman[16]).

Figure 12 shows a 3d computer simulation of the metal atom deposition process on a pI substrate, by Silverman.[16] At one-quarter metal atom monolayer deposition, a highly diffuse interface has formed. The 2d view of this interface can be compared with those in Figures 3–5. Silverman also simulates the annealing process and finds that the aggregation of metal atoms with strong interactions into clusters considerably reduces the ramified nature of the interface. From a plot of log mass versus log radius, he

finds that the clusters have a fractal dimension of 2.98, which reflects their globular compact structure. On the other hand, the aggregation of clusters with weak interactions gives a fractal dimension of 1.5 ± 0.10.

Mazur et al.[17-19] formed diffuse silver–polyimide interfaces by electrochemical deposition. A silver ion solution was permitted to diffuse into a polyimide film, and the ions were reduced from Ag^+ to Ag^0 on the cathode side of the film. The results are shown in Figure 13. A transmission electron micrograph (TEM) of an 800-Å slice of the film is shown where the space bar represents 1000 Å. This figure presents a near 2d view of a 3d diffusion field. The particles form a conducting black strip with a highly diffuse region of silver particles. The close-up view of the particles in Figure 13 shows a size distribution from about 50 to 500 Å.

Mazur found that the metal layer could not be delaminated from the polymer substrate and could only be removed by abrasion. This indicated excellent adhesion at the polymer–metal interface. However, for such diffuse interfaces, one may ask, where is the interface? The fractal interface analysis suggests that it is the fractal diffusion front which represents the outer frontier of connected silver which can offer mechanical resistance. The adhesion should be enhanced by the very rough diffusion front, which would provide considerable mechanical interlocking in addition to a high surface contact area for bonding.

Comparing Figure 3 with Figure 13, we can make the following comparison: The black area represents the percolating conducting region. The white region represents a polymer–metal interphase region adjacent to the conducting metal strip which will have unique mechanical and electrical properties. For example, one can expect to have a gradient of mechanical moduli and thermal expansion coefficients in this interphase region.

However, there is a potentially serious problem for electronic materials with such diffuse interfaces. The technology shown in Figures 11 and 13 is often used to make high-speed circuits, e.g., in computers. For such a system, the delay time for the electrical signal or pulse time t_p is determined by

$$t_p \sim h\sqrt{K'} \tag{31}$$

where h is the length of the strip and K' is the dielectric constant of the polymer substrate in contact with the conducting strip.

Polymer dielectrics with large K' values slow the electric signal because the electric field of the pulse induces a field of opposite sign in the dielectric which slows it down. The magnitude of the opposing field is determined by the polarizability of the polymer molecules. The dielectric constant, in the low-frequency limit, is proportional to the refractive index of the polymer. A value of $K' = 1$ is ideal but can only be approximated using air with suspended wire, or aerogel, technology. Typical K' values of polymer dielectrics in electronic materials are in the range of 2–4. Air can be used as the dielectric in suspended wire technology and in aerogels, but each has its unique application problems. Equation 31 is used in high-speed computer design by making the distance h between contact points as small as possible using submicron VLSI technology and using dielectric materials with very low K' values, such as PI and poly(tetrafluoroethylene) (Teflon). However, with polymer–metal interfaces as shown in Figures 12 and 13, the polymer material immediately adjacent to the conducting metal strip is now highly modified by the nonconducting dissolved metal particles and the K' value may be substantially increased above its design value.

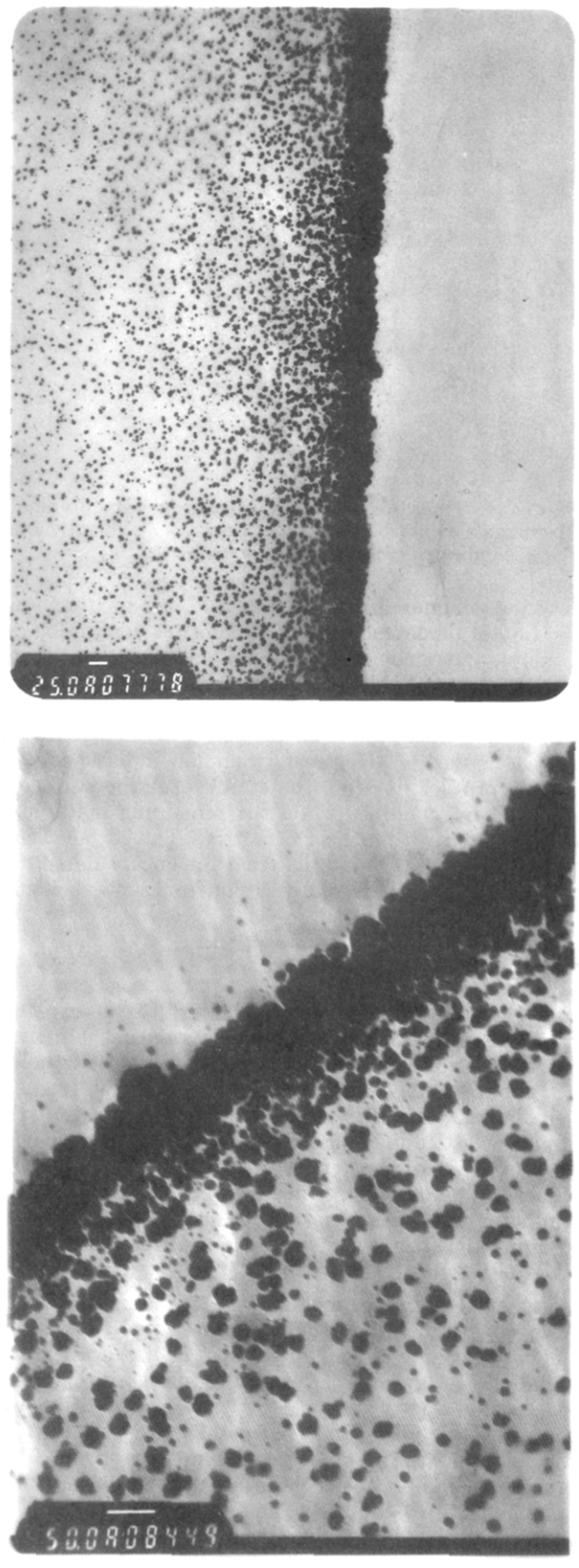

Figure 13. (a) Transmission electron micrograph of a polyimide film containing a concentration gradient of electrochemically deposited silver particles. The film for TEM analysis was obtained by taking a 1000-Å slice through the interface. The bar marker is 1000 Å. (b) A higher magnification of a similar Ag–PI interface shows a distribution of silver particles sizes ranging from about 50 to 500 Å (courtesy of Mazur et al.[17]).

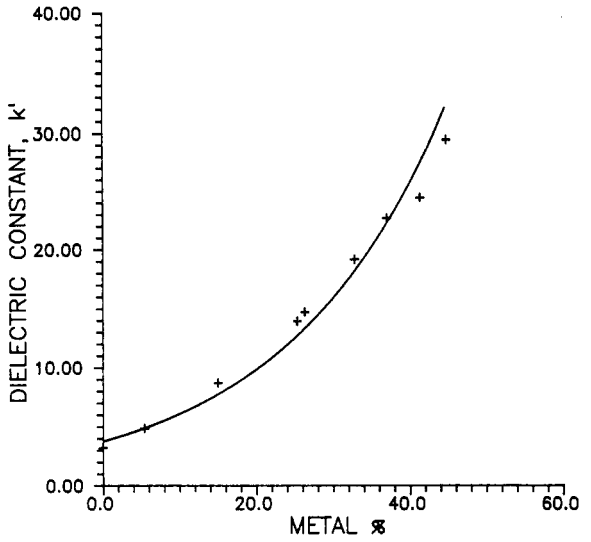

Figure 14. Dielectric constant vs aluminum powder volume fraction in a polyester composite. Data were obtained at 20 °C and 100 kHz (data of Berger and McCullough[20]).

Figure 14 shows the effect of a uniform concentration of aluminum powder on the dielectric constant of a polyester resin. We made the plot from dielectric data obtained by Berger and McCullough,[20] using composite samples at 20 °C and 100 kHz. The K' value increases from 3.2 at 0% metal to about 30 at 45% metal. The conductivity percolation threshold for this 3d system is in the vicinity of 31% by volume metal. At this concentration, $K' \approx 20$, or about 6 times its initial value. We cannot apply these results totally to the polymer–metal interface with a metal concentration gradient, but we can expect similar changes to occur locally. Thus, the fractal nature of the interface may provide an advantage in mechanical properties but could have adverse effects on some electrical properties and improve others at certain operating frequencies and current densities.

The thermal properties of fractal polymer–metal interfaces have not been analyzed. One of the major factors in the failure of polymer–metal interfaces in electronic and composite materials is the difference in thermal expansion coefficients (about a factor of 10). With large temperature changes, often encountered during processing or use, significant interfacial stresses develop which can result in failure of the material. The sharper the interface, the greater the mismatch and interfacial stress. Conversely, the more diffuse the interface, the lower will be the stress. We expect that the interfacial stresses, s_{ij}, are inversely proportional to the fractal diffusion front width σ_f and proportional to the temperature difference $(T_2 - T_1)$ and thermal expansion coefficient difference between polymer and metal $(\alpha_p - \alpha_m)$, such that[21]

$$s_{ij} \approx (T_2 - T_1)(\alpha_p - \alpha_m) L_d^{-\nu/(\nu+1)} \tag{32}$$

where L_d is the diffusion length and ν is the critical exponent for the percolation correlation length. Thus, fractal interfaces should be more stable with respect to temperature changes with increasing L_d values.

Fractal Dimension of a Silver–Polyimide Interface. We analyzed the silver–polyimide interface TEM micrograph shown in Figure 13. Since the TEM image was not on a digital data file, a procedure to capture the image to machine-readable form was necessitated. Further image analysis was required prior to submitting the data to the fractal dimensional analysis (FDA) software. The FDA software used in Figures 3–5, works with a two-dimensional binary lattice, while the captured data is initially encoded with lattice site values ranging from 0 to 255.

The first step in the process was to convert the TEM image to a computer file using a light table and a charge-coupled device video camera. The camera was connected to a Truevision Vista board in an IBM PC/AT. Utilizing Truevision's Vista-Tips software, a white scale image was obtained at a resolution of 756 × 486 pixels. Next the captured image was rescaled via color imaging and histogram analysis from the original set of values (0–255) to a resolved range of 0–7. This process was accomplished using an IBM 7350 image processor with Hlips image analysis software.

The rescaled image was then used as an input file to the FDA software which was modified to allow for selective dichotomization of the cell values. This modification provided the ability to reexamine the image with different levels of occupation. Presented in Figure 15 are three analyses of the PI–Ag image which vary with respect to how stringent the criteria for cell occupation was set. The connected metal region (black) is separated from the polyimide phase which is interspersed with nonconnected metal particles (white), separated by the frontier (gray).

The fractal dimension of the frontier was found to be sensitive to the image resolution and varied in Figure 15 from 1.492 to 1.619. Using the human eye to locate the position of the front from Figure 13, we obtained the result shown on the bottom of Figure 1, where only the percolating part of the metal is shown and the front is represented by the leading edge. By digitizing this image and using the FDA software, we obtained the diffusion front and front density profile shown in Figure 16. The breadth or span of the profile $B = 42$ digitized units, which corresponds to about 3000 Å on the real silver interface (Figure 13). The mass of the frontier $N_f = 1056$ in Figure 16. The width of the front was determined from a Gaussian analysis using

$$\sigma_f = N_f/(N_{max}\sqrt{2\pi}) \tag{33}$$

where N_{max} is the number of particles at the peak. From Figure 16, we have $N_{max} = 58$ and $N_f = 1056$ such that $\sigma_f = 7.26$. The ratio $B/\sigma_f = 6.06$ which is in excellent agreement with theory and simulation for this lattice length. The position of the front occurs at $X_f = 37$ (Figure 16 has a 15-point offset on X_f), resulting in a diffusion length $L_d = 98$.

A plot of the diffusion front mass (in Figure 16) as a function of radius gave a fractal dimension $D = 1.73$ (shown in Figure 17), which is in very good agreement with theory and computer simulations of Sapoval et al. The fractal dimension is quite sensitive to the resolution used to analyze the image. If we take a true frontier with $D = 1.75$ and analyze it with decreasing resolution, then the fractal dimension will decrease to a lower bound determined by a self-avoiding walk (SAW) such that $D = 1.33$.[22] As the resolution decreases, the "harbors" and small bays close up and are not detected and the front loses its ramification and eventually converges to a SAW with a lower fractal dimension. Figure 17 also shows the result of an image analysis of a TV image of a computer-simulated diffusion field which had a true fractal dimension of $^7/_4$. The image analysis method slightly reduces the fractal dimension, but very little difference is seen between the two data sets in Figure 17.

From the image analysis of the Ag–PI interfaces shown in Figure 15, we can evaluate several quantitative aspects of the frontier theory. The frontier equations will be used

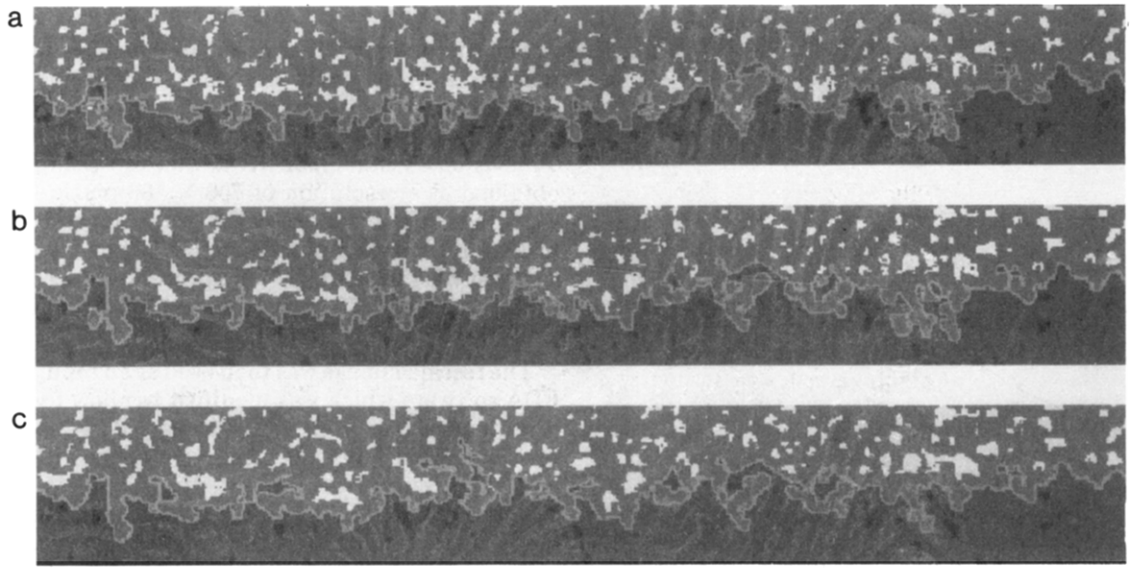

Figure 15. Image analyses of the Ag–PI interface (from Figure 13). The gradient percolation analysis of the images (a–c) obtained under varying resolution is given in Table II.

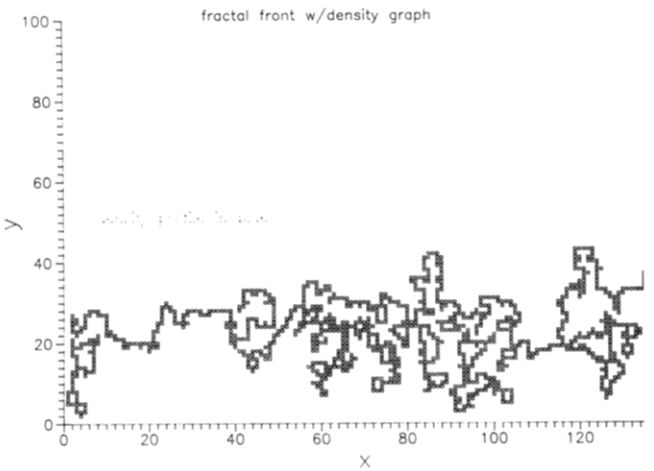

Figure 16. Diffusion front of the Ag–PI interface (from Figure 13) (analysis in Table II, image d).

in the following forms:

$$N_f = 0.92L_d^{1-1/D} \quad (34)$$

$$\sigma_f = 0.46L_d^{1/D} \quad (35)$$

$$B/\sigma_f \approx 6 \quad (36)$$

$$L_d = 2.645x_f \quad (37)$$

$$N_f\sigma_f/(LL_d) = 0.44 \quad (38)$$

$$S = 2.4L_d/B \quad (39)$$

Equation 38 examines the invariant ratio of the front factors in the above relations since the exponents cancel. This relation also suggests that the number of front particles per box of width σ_f is proportional to the diffusion length L_d. We proceed by taking the experimental values of N_f, σ_f, B, and D, and using x_f to determine L_d, we compare them with the theoretical values using the above equations. The experimental value of D was used in each equation to obtain the theoretical prediction. The results are shown in Table II.

The results show considerable support for the general theory. In particular, it should be noted that the exact fractal dimension of 1.75 is not necessary to describe the quantitative aspects of the interface. The exponents for

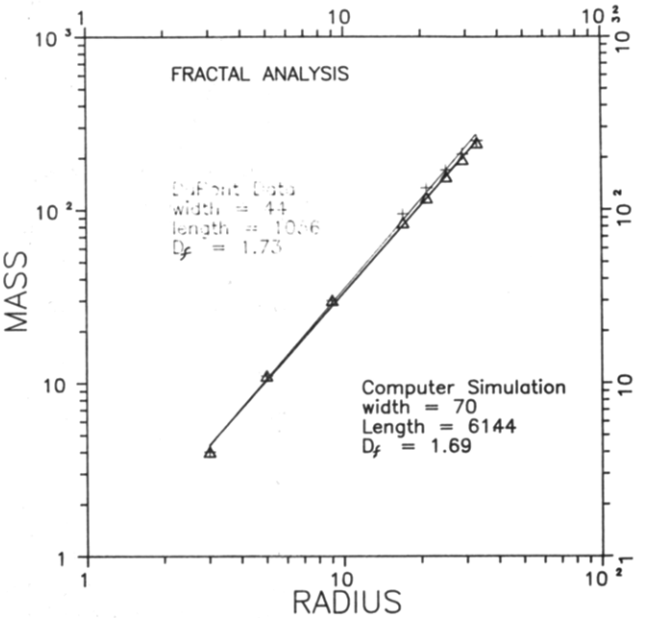

Figure 17. Fractal analysis mass vs radius of a Ag–PI diffusion front: (–+–) Analysis of Ag–PI Du Pont data in Figure 16; (–Δ–) image analysis of computer-simulated frontier with $D = 1.75$.

N_f, σ_f, etc., can be expressed in terms of the observed fractal dimension.

Fractal Polymer–Polymer Diffusion Fronts

In this section, we consider the nature of the interface formed by joining of two identical pieces of amorphous polymer. Such is the case in welding of polymers in the melt, lamination of composites, coalescence of powder and pellet resins, drying of latex paints, internal weldlines formed during injection and compression molding, tack of uncured elastomers, and a multitude of processing operations where interdiffusion is required to develop full strength at an interface.[1,2] The analysis of the fractal nature of amorphous polymer diffusion fronts is complicated by the interpenetrated nature of the random-coil chains allowing several statistical segments or monomers to occupy a single lattice site. The computer simulation of polymer diffusion on 2d and 3d lattices was done in a manner so as to keep track of both the occupied number

Table II. Analysis of the Ag-PI Interface

property	image a	image b	image c	image d
front position x_f	26	32	37	37
diffuse length L_d	68.77	84.64	97.86	98
lattice length L	486	486	486	136
fractal dimen D	1.492	1.619	1.572	1.73
$1/D$	0.670	0.618	0.636	0.578
$1 - 1/D$	0.330	0.382	0.364	0.422
front span B	43	43	52	44
front width σ_f	8.453	8.563	8.664	7.33
theory σ_f	7.83	7.14	8.488	6.511
B/σ_f	5.1	5.0	6.0	6.0
B/σ_f theory	6	6	6	6
front length N_f	2015	2013	2147	1056
theory N_f	1806	2436	2371	866
$N_f\sigma_f/LL_d$	0.51	0.42	0.39	0.58
$N_f\sigma_f/LL_d$ theory	0.44	0.44	0.44	0.44
Sapoval no. S	3.84	4.72	4.52	5.34

of lattice sites N_L and the total number of monomers in the multiple occupied lattice sites N_m.

The algorithm used for monomer diffusion fronts was also used for polymers where the connectivity under gradient percolation conditions was examined in terms of connected lattice sites and the diffusion front was identified as the boundary between connected and nonconnected lattice sites. The diffusion front could then be quantified either in terms of the occupied lattice sites, as in the monomer case, or in terms of the total number of monomers where multiple occupancy per lattice site was permitted for random-walk chains. Individual monomers on polymer chains do not occupy the same space, of course, but the statistical segments, or equivalent random-walk steps of the real chain, representing up to about 20 monomers per step, highly interpenetrate each other. The multiple occupation concept is even further amplified if one considers mechanical connectivity in terms of entanglements, where the average network strand representing the amorphous polymer network is determined by the critical entanglement molecular weight, M_c.

The interdiffusion of polymer chains can be divided into four dynamic regions,[23,24] which can be described in terms of characteristic length scales at characteristic relaxation times. These are (1) Rouse relaxation of entanglement lengths resulting in diffusion lengths $L_d \approx 0.8R_e$, where R_e is the radius of gyration of the entanglement segment; (2) Rouse relaxation of the whole chain in a tube of topological constraints such that $L_d \approx R_e(M/M_e)^{1/4}$, where M_e is the entanglement molecular weight; (3) reptation of the whole chain occurs such that $L_d \approx 0.8R_g$, where R_g is the radius of gyration of the whole chain; and (4) long-range Fickian diffusion of the whole chain occurs with $L_d \gg R_g$ and the chains essentially behave as Brownian particles exhibiting center-of-mass motion.

Our principal interest here is to examine the largest region of value in welding of interfaces, namely, the reptation region with $L_d < R_g$ and times t less than the reptation time T_r, followed by the transition to normal Fickian diffusion at $L_d > R_g$ and $t > T_r$. In this study, the diffusion length L_d will be determined in terms of the average monomer interdiffusion distance $\langle X \rangle$, with consideration for multiple occupation of lattice sites.

Diffusion Fronts of Polymer Interfaces with Reptation. Interdiffusion of polymer chains was simulated using random-coil chains with a reptation algorithm. In this algorithm, a random walk is moved by a process which randomly selects a chain end which is moved one step in a random direction on a 2d or 3d lattice and subtracts a monomer from the other end. The de Gennes reptation

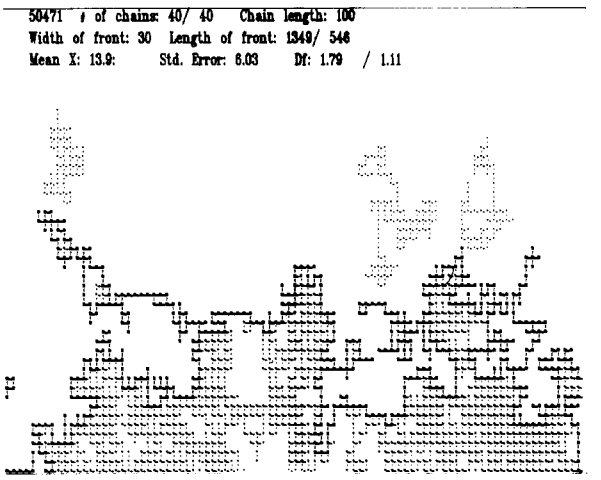

Figure 18. Polymer–polymer interface (one side) simulation on a 2D lattice. The interface was formed by reptation of random-coil interpenetrated chains of length 100 steps.

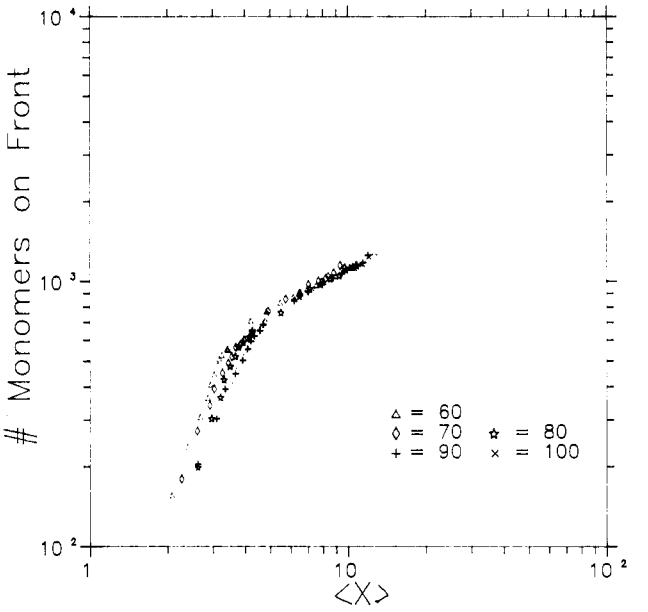

Figure 19. Number of monomers on the polymer diffusion front N_m plotted vs the average monomer diffusion depth $\langle X \rangle$, for chains of length 60–100 steps.

mechanism results in Brownian motion of the center of mass of the chain but with correlated motion for the chain monomers at times $t < T_r$. Figure 18 shows a typical ramified diffusion field for the polymer interface in 2d. The diffusion front was obtained using the same technique employed for monomer diffusion. The front is potentially more ramified initially due to the connectivity of monomers within a given chain. At $t < T_r$, most of the chains contribute to the front and very few chains have escaped to longer diffusion distances.

Figure 19 shows the number of monomers on the diffusion front, N_m, as a function of the average monomer interdiffusion distance, $\langle X \rangle$, for random-coil chains of molecular weight ratios M/M_e, ranging from 60 to 100. Two regions of behavior are observed: (1) at $\langle X \rangle < R_g$ and $t < T_r$ and (2) at $\langle X \rangle \gg R_g$ and $t \gg T_r$.

For $t < T_r$, the front is discontinuous since the concentration profile for reptating chains has a gap or discontinuity at $p(0,t)$.[25-27] Thus, the time dependence of N_m can be well approximated by summing average contributions from single chains as

$$N_m \approx n(t)\,\langle X \rangle^{d-1} \tag{40}$$

where $n(t)$ is the number of chains crossing the unit area

(3d) or unit length (2d) of the initial interface plane and $\langle X \rangle$ is the average monomer interpenetration distance. When $d = 2$, the contribution to the front from a single random-walk chain is the span of the walk, which has the same scaling law as $\langle X \rangle$. In 3d, the individual chain contribution to the front is determined by the average interpenetration contour length $l(t)$, which is proportional to $\langle X \rangle^2$.

To evaluate eq 40 in terms of the fractal diffusion front theory, we need to convert from a time dependence to a diffusion length dependence of N_m. The average monomer interdiffusion length $\langle X \rangle$ is determined by[1-3]

$$\langle X \rangle \approx R_g(t/T_r)^{1/4} \quad (t < T_r) \tag{41}$$

and

$$\langle X \rangle \approx R_g(t/T_r)^{1/2} \quad (t > T_r) \tag{42}$$

where the crossover from $t^{1/4}$ to $t^{1/2}$ diffusion occurs near T_r. In these relations, the reptation time has a molecular weight dependence given by $T_r \sim M^3$ and a radius of gyration $R_g = (M/6M_e)^{1/2}$.

The number of chains crossing the interface is determined by the initial distribution of the chain ends. If the chain ends are uniformly distributed in space, we have shown that the number of chains crossing is given by[1]

$$n(t) \approx n_\infty(t/T_r)^{1/4} \quad (t < T_r) \tag{43}$$

where $n_\infty \sim M^{-1/2}$ is determined at T_r. In terms of the monomer diffusion depth $\langle X \rangle$,

$$n(t) \sim \langle X \rangle / M \tag{44}$$

Thus, the number of monomers on the front is

$$N_m \sim \langle X \rangle^d / M \quad (t < T_r) \tag{45}$$

In the special case where the chain ends are segregated at the interface at $t = 0$, then

$$n_s(t) \sim t^0 M^{-1/2} \quad (t < T_r) \tag{46}$$

and the number of monomers on the front is

$$N_{ms} \sim \langle X \rangle^{d-1} / M^{3/2} \quad (t < T_r) \tag{47}$$

When $t \gg T_r$ and $\langle X \rangle \gg R$, all correlated motion effects are lost and the polymer diffusion front should attain characteristics similar to the monomer diffusion front with

$$N_m \sim \langle X \rangle^{1-1/D} \tag{48}$$

where D is the fractal dimension with $d = 2$.

Figure 19 shows a plot of $\log N_m$ vs $\log \langle X \rangle$ for simulated interdiffusion of reptating random walks in 2d with molecular weight ratios M/M_e in the range 60–100 and with a uniform initial distribution of chain ends. At $t < T_r$, the plot on a log–log scale has a slope of about 2 for all molecular weights, and at constant $\langle X \rangle$, N_m varies approximately as the inverse of M, in agreement with eq 45. The latter relation contrasts with the monomer diffusion front with $N_f \sim \langle X \rangle^{0.43}$.

At times less than the reptation time, the diffusion front, though very rough, is not considered to be fractal since the criterion of self-similarity is not obeyed at length scales less than $\langle X \rangle$ due to discontinuities in the interface plane. This concept may need to be modified when consideration is given to short-range segmental motion. Rouse-like motion of short-chain segments was not considered in this simulation, and the results reflect only the concentration profile for monomers on the primitive path of the reptating chain. The time-dependent scaling law for N_m at $t < T_r$ is identical to that for bridges, $p(t) \sim t^{1/2}M^{-3/2}$.

Table III. Polymer Fractal Dimensions

mol wt	front mass fractal $D(m)$	lattice site fractal $D(L)$
60	1.77	1.53
70	1.78	1.56
80	1.63	1.48
90	1.76	1.60
100	1.72	1.62

In three dimensions, at $t < T_r$, the number of monomers on the diffusion front is well approximated by the total number of monomers which have diffused across the interface $N(t)$. Comparing with the 2d case, the number of chains crossing the interface $n(t)$ is the same in 3d, but the single-chain contribution to the front is proportional to $\langle X \rangle^2$, such that[1-3]

$$N(t) \approx R_g/2(t/T_r)^{3/4} \quad (t < T_r) \tag{49}$$

Substituting for $\langle X \rangle$ from eq 41, we have the 3d result

$$N_m \sim \langle X \rangle^3 / M \tag{50}$$

The latter relation has been observed by Whitlow and Wool[28] using a SIMS analysis of a HPS–DPS interface. Thus, in 3d, the polymer interface is extremely rough compared to the monomer diffusion case where $N_m \sim \langle X \rangle$.

Polymer Diffusion Fronts at $\langle X \rangle \gg R_g$. At $t = T_r$, since $\langle X \rangle \sim M^{1/2}$, $N_m(T_r)$ becomes independent of molecular weight as indicated for the 2d case. This effect is seen in Figure 19 where N_m for all molecular weights converges on a common line at long times. In this region, the fine structure of the chain disappears in the dynamic sense and the motion of the chains is represented by simple center-of-mass motion. Thus, when polymer chains behave as monomers at long times, we expect to recover the simple result for the number of monomers on the diffusion front at $t \gg T_r$, as

$$N_m \sim \langle X \rangle^{0.43} \tag{51}$$

The latter result is shown in Figure 19 where the slope converges to 0.43 for all molecular weights at $\langle X \rangle \gg R_g$ of each chain.

Table III shows the results of the mass–radius fractal analysis of the polymer diffusion fronts as a function of molecular weight for the two cases

$$N_m \sim R^{D(m)} \quad \text{(mass fractal)} \tag{52}$$

$$N_L \sim R^{D(L)} \quad \text{(lattice site fractal)} \tag{53}$$

where N_m is the total number of monomers on the front with consideration for multiple occupancy of lattice sites due to chain interpenetration, N_L is the number of occupied 2d lattice sites on the diffusion front, independent of multiple occupation, and $D(m)$ and $D(L)$ are the corresponding fractal dimensions. The analysis was done in the time region $t \approx 10T_r$ and length scales $R \gg R_g$ of each molecular weight, such that all correlated motion effects were lost and the diffusion profile was Fickian. It can be seen (Table III) that the fractal dimension for the total mass of monomers on the diffusion front $D(m) \approx 1.75$ for all molecular weights and compares well with the monomer diffusion case where $N_f \sim R^{7/4}$ in 2d. Interestingly, the fractal dimension of the diffusion front evaluated with respect to the occupied lattice sites is consistently lower, with $D(L) \approx 1.57$. This may be due to a polymer connectivity effect between lattice sites, causing a smoothing of the fractal structure and resulting in a lower fractal

dimension. In 3d, the fractal dimension of the diffusion front $D(m)$ is about 2.5 at long diffusion times, similar to the monomer case.

Summary

When diffusion occurs at an interface, the concentration profile $p(x,t)$ varies smoothly as a function of the one-dimensional depth x. However, when the diffusion process is viewed in two or three dimensions, the interface is not smooth and is very rough. The random nature of diffusion permits the formation of complex structures with fractal characteristics. In this paper, we used gradient percolation theory developed by Sapoval et al. to examine the structure and properties of diffuse interfaces formed by metallization of polymer substrates and welding of symmetric amorphous polymer interfaces. Gradient percolation separates the connected from the nonconnected region of the diffusion field. The edge of the connected region is the (fractal) diffusion front.

We first used computer simulation to examine the monomer–monomer interface structure in terms of the diffusion front's width σ_f, length N_f, position X_f, breadth B_f, fractal dimension D, and "noise" in these properties, $\delta\sigma_f^2$, δN_f^2, δX_f^2, and δB_f^2, respectively, as a function of the diffusion length L_d. We obtained the following results: width, $\sigma_f \sim L_d^{1/D}$, $\delta\sigma_f^2 \sim L_d^{3/D}$; front length, $N_f \sim L_d^{1-1/D}$, $\delta N_f^2 \sim L_d^{2-1/D}$; position, $X_f \sim L_d$, $\delta X_f^2 \sim L_d^{2-1/D}$; breadth $B_f \approx 6\sigma_f$, $\delta B_f^2 \sim L_d^{(2-1/D)}$, where $D = {}^7/_4$.

The simulation results compared very favorably with an experimental image analysis of diffuse silver–polyimide interfaces. Gradient percolation theory gave an excellent description of the diffuse metal interface, where all properties could be described by the apparent fractal dimension of the diffusion front.

For welding of polymer–polymer interfaces, we examined the diffusion front for reptating chains of molecular weight M and found that the interface became fractal at diffusion distances L_d greater than the radius of gyration $R_g \sim M^{1/2}$ and at times t longer than the reptation time T_r. At $t < T_r$ and $L_d < R_g$, self-similarity was lost due to the correlated motion of the chains creating "gaps" in the interface. However, the interface was very rough and the diffusion front was determined by $N_f \sim L_d^d/M$, where d is the dimensionality ($d = 2$ or 3). When $L_d \gg R_g$, the polymer diffusion front behaved as the monomer case with $N_f \sim L_d^{(1-1/D)}$. The fractal nature of diffuse interfaces plays an important role in controlling the physical properties of polymer–polymer and polymer–metal interfaces.

Acknowledgment. The authors are grateful to the Air Force Office of Scientific Research, Grant AFOSR-90-0242, via the Center for Cement Composite Materials at the University of Illinois, IBM for their support of Research in Materials and Processing Science at the University of Illinois (UI), and the Federation of Advanced Materials Industries (UI). The research was supported in part by the National Center for Supercomputing Applications, University of Illinois. Appreciation is expressed to Joe Futrelle, Jonathan Faiman, and Michael Grady for their assistance with the software development and Image Analysis. R.P.W. particularly expresses thanks to Professor Bernard Sapoval, Ecole Polytechnique, Paris, for many fruitful discussions during a sabbatical visit to Paris.

References and Notes

(1) Wool, R. P. *Structure and Strength of Polymer Interfaces*; Hanser Press: 1994, New York, in press.
(2) Wool, R. P.; Yuan, B.-L.; McGarel, O. J. *Polym. Eng. Sci.* **1989**, *29* (19), 1340.
(3) Wool, R. P. In Dynamics and Fractal Structure of Polymer Interfaces. *New Trends in Physics and Physical Chemistry of Polymers*: Lee, L.-H., Ed.; Plenum Press; New York, 1989; p 129.
(4) Sapoval, B.; Rosso, M.; Gouyet, J. F. *J. Phys. Lett.* **1985**, *46*, L149.
(5) Ziff, R. M.; Sapoval, B. *J. Phys. A: Math. Gen.* **1986**, *19*, L1169.
(6) Kolb, M.; Gouyet, J. F.; Sapoval, B. *Europhys. Lett.* **1987**, *3*, 33.
(7) Rosso, M.; Sapoval, B.; Gouyet, J. F. *Phys. Rev. Lett.* **1986**, *57*, 3195.
(8) Sapoval, B.; Rosso, M.; Gouyet, J. F. In Fractal Interfaces in Diffusion, Invasion and Corrosion. *The Fractal Approach to Heterogeneous Chemistry*; Avnir, D., Ed.; John Wiley and Sons, Ltd.: New York, 1989.
(9) Wool, R. P.; Long, J. M. Structure of Diffuse Polymer Metal Interfaces. *Polym. Prepr. (Am. Chem. Soc., Div. Polym. Chem.)* **1990**, *31* (2).
(10) Sapoval, B.; Rosso, M.; Gouyet, J. F.; Colonna, J. F. *Solid State Ionics* **1986**, *18–19*, 21.
(11) Desai, P. G.; Young, J. F.; Wool, R. P. In *Advanced Cementitious Systems: Mechanisms and Properties*; Glasser, F. P., Pratt, P. L., Mason, T. O., Young, J. F., McCarthy, G. J., Eds.; Materials Research Society: Pittsburgh, PA, 1992, Vol. 245.
(12) Peanasky, J. S.; Long, J. M.; Wool, R. P. *J. Polym. Sci., Part B: Polym. Phys. Ed.* **1991**, *29*, 565.
(13) Wool, R. P.; Raghavan, D.; Billieux, S.; Wagner, G. C. In Statics and Dynamics in Biodegradable Polymer-Starch Blends. *Biodegradable Polymers and Plastics*; Vert, M., Feijen, J., Albertsson, A., Scott, G., Chiellini, E., Eds.; Royal Society of Chemistry: London, 1992; p 111.
(14) Peddada, S. R.; Robertson, I. M.; Birnbaum, H. K. *J. Mater. Res.*, in press.
(15) Ho, P. S.; Haight, R.; White, R. C.; Silverman, B. D.; Faupel, F.; Chapter 14, In *Fundamentals of Adhesion*; Lee, L.-H., Ed.; Plenum Press: New York, 1991.
(16) Silverman, B. D. *Macromolecules* **1991**, *24*, 2467.
(17) Masur, S.; Reich, S. *J. Phys. Chem.* **1986**, *90*, 1365.
(18) Mazur, S.; Lugg, P. S.; Yarnitzky, C. *J. Electrochem. Soc.* **1987**, *134* (2), 346.
(19) Manring, L. E. *Polym. Commun.* **1987**, *28*, 68.
(20) Berger, M. A.; McCullough, R. L. *Compos. Sci. Technol.* **1985**, *22*, 81.
(21) Wool, R. P. Fractal Polymer Interfaces. *Proceedings of Fractals In Engineering*, *31*; Ecole Polytechnique, June 3, 1992.
(22) Grossman, T.; Aharony, A. *J. Phys. A* **1986**, *19*, L745; **1987**, *20*, L1193.
(23) Doi, M.; Edwards, S. F. *Faraday Trans.* **1978**, *2*, 1789.
(24) de Gennes, P.-G. *J. Chem. Phys.* **1971**, *55*, 572.
(25) de Gennes, P.-G. *C. R. Acad. Sci., Paris* **1981**, *292*, 1505.
(26) Zhang, H.; Wool, R. P. *Macromolecules* **1989**, *22*, 3018.
(27) Kim, Y.-H.; Wool, R. P. *Macromolecules* **1983**, *16*, 1115.
(28) Whitlow, S. J.; Wool, R. P. *Macromolecules* **1991**, *24*, 5929.